Titania-Carbon Nitride Interfaces in Gold-Catalyzed CO Oxidation

Pablo Jiménez-Calvo, Loïc Michel, Valérie Keller, Valérie Caps

Titania-Carbon Nitride Interfaces in Gold-Catalyzed CO Oxidation

Pablo Jiménez-Calvo,[†] Loïc Michel, Valérie Keller, Valérie Caps*

ICPEES (Institut de Chimie et Procédés pour l'Energie, l'Environnement et la Santé), University of Strasbourg / CNRS UMR 7515, 25 rue Becquerel, 67087 Strasbourg Cedex 02, France

ABSTRACT: Gold-catalyzed CO oxidation is a reaction of both practical and fundamental interest. In particular, rate-determining oxygen activation pathways have attracted a lot of attention. They have been found to depend on the surface chemistry of the catalyst support, titania providing the most active catalysts and carbon nitride leading to inactive catalysts. Here we show that C_3N_4-TiO_2 composites with rather similar surface chemistries can be engineered by using titania nanotubes as hard templates and by performing the polycondensation of melamine and dicyandiamide in air and in ammonia. By varying the C_3N_4 content from 2 to 75wt.%, the mesoporosity can be tuned from 8 nm to 40 nm. A systematic study of CO oxidation turnover numbers in the absence and in the presence of hydrogen over the composites loaded with well-calibrated, 2-4 nm gold nanoparticles clearly shows that (1) the chemical composition of the support surface has much less impact on PROX than on dry CO oxidation (2) NH_2-terminated supports are as active as OH-terminated supports in PROX (3) hydrogen/water-mediated CO oxidation pathways are active on C_3N_4-based Au catalysts, (4) PROX activity requires a rather large porosity (40 nm), which suggests the involvement of much larger intermediates than the usually postulated peroxo-type species.

KEYWORDS: carbon nitride, titania, composites, gold catalysts, PROX, porosity, surface chemical composition

INTRODUCTION

Au/TiO2 is a well-known catalyst for the low temperature oxidation of CO. Such gold-catalyzed oxidation reaction involves peculiar oxygen activation pathways,[1] as compared with the redox version over transition metal oxides.[2-4] Although oxygen can theoretically be activated on very small gold nanoparticles (Au NPs), the direct adsorption of oxygen on Au NPs of the typical catalytic size, i.e. 3-5 nm, has a much higher barrier.[5] Gold oxidation catalysis thus relies on the presence of an "active" support according to Schubert's terminology.[6] Amongst them,[7] titania is a benchmark. It has proven to exhibit the most suitable surface chemistry[8-11] which allows for complex oxygen activation pathways[12-14] in dry CO/O2 feeds. Non-reducible, hydroxyl-terminated metal oxide supports may be good alternatives when water or hydrogen is present in the feed, due to oxygen activation pathways via surface hydroxyl functions,[15] which are enhanced by the presence of hydrogen and water. These make efficient PROX catalysts (preferential oxidation of CO in excess hydrogen).[16-18] In general, hydrophilic oxides[19] are suitable supports for gold PROX catalysts, due to water-mediated oxidation pathways.[20-23]

The surface chemical composition of the inorganic support on which Au NPs are dispersed is thus a key parameter which determines the reactivity of gold catalysts in CO oxidation,[24] like in many other reactions.[25] In this regard, C_3N_4 yields inactive gold catalysts because of its inadequate surface chemistry towards oxygen activation under hydrogen-free and water-free conditions.[26] However, a heterostructured TiO_2–C_3N_4 support was reported to yield an active gold catalyst for the PROX reaction.[27]

Composites of titania and carbon nitride are more widely studied in photocatalysis,[28-35] due to the ability of both components to form a heterojunction which increases charge carrier lifetime, extends the absorption wavelength range and thus yields photocataytic properties in the visible range. However it was found that the formation of a suitable heterojunction is critically dependent on the TiO_2/C_3N_4 interface. We have recently shown that a suitable interface could be obtained by performing the polycondensation of C_3N_4 precursors in the presence of pre-formed titania crystallites in air. Such materials exhibited, after additional gold nanoparticle deposition, a state-of-the-art behavior in challenging water photoreduction to hydrogen.[36,37] Besides, we recently reported that the surface chemistry of C_3N_4 (as well as its crystallinity, morphology and porosity) could be tuned by the atmosphere of the polycondensation process leading to its synthesis. In particular, the specific surface area and porosity of C_3N_4 could be markedly enhanced by performing polycondensation in ammonia instead of air.[38] The importance of the porosity of functional materials designed for CO_2 and N_2 reductions has recently been highlighted.[39] Yet there is no report to date concerning the importance of the porosity of gold PROX catalysts.

By directing the growth of C_3N_4 using titania nanotubes as hard template, by tuning the porosity of the composite *via* both the C_3N_4/TiO_2 composition and the polycondensation atmosphere (air vs. ammonia) and by using the resulting C_3N_4-TiO_2 composites as supports for

Au NPs, we here show (1) that PROX activity is observed on Au/C3N4 due to active hydrogen/water-mediated oxidation pathways and (2) that the gold-catalyzed CO PROX reaction is critically dependent on the porosity of the support.

EXPERIMENTAL

Materials

Melamine ($C_3H_6N_6$, 99%, Sigma Aldrich), dicyandiamide ($C_2H_4N_4$, 99%, Sigma Aldrich), AEROXIDE® TiO_2 P25 (Evonik Industries), sodium hydroxide (NaOH, ≥98%, Sigma Aldrich), hydrochloric acid (HCl, fuming ≥37%, Sigma Aldrich), chloroauric acid ($HAu^{III}Cl_4$) (≥ 99.9% trace metals basis, Alfa Aesar), sodium borohydride (≥98%, Sigma Aldrich), methanol (CH_3OH, ≥99.6%, Sigma Aldrich), ethanol (CH_3CH_2OH, ≥96%, Sigma Aldrich), were used without further purification.

Synthesis of the supports

Graphitic carbon nitride (g-C_3N_4) was synthesized via thermal polycondensation of an equimolar relationship of melamine (M) and dicyandiamide (D) as described elsewhere.[36] In brief, M and D precursors were mixed in an agate mortar and were placed in an alumina crucible, covered with a lid. Thermal polycondensation was carried in a tubular furnace at 550 °C for 3 h (ramp of 5 °C min^{-1}) with a continuous flow of 100 mL min^{-1} of the designated atmosphere, i.e. air or NH_3.

The materials are referred to as C_3N_4 (*atm*), where *atm* stands for the atmosphere of the polycondensation treatment (air or NH_3).

Titania nanotubes (TiO_2-NT) were synthesized via hydrothermal method as described elsewhere.[40] In brief, P25 and NaOH (10 M) aqueous solution were mixed and stirred for 1 h in a Teflon vessel. The solution was then transferred in a Teflon reactor, covered with a stainless steel jacket. A thermal treatment was applied (130 ◦C for 48 h) in a stove. After cooling the solution was washed with deionized (DI) water, filtrate and dry at 100 ◦C for 2h. The solution was re-dispersed to obtained a pH = 2, using HCl (1 M) and stir for 18h. A final washing with DI water until neutrality took place. Then, it was filtered and dried at 110 ◦C for 10 h. Finally, a calcination step was applied at 380 ◦C for 2 h (ramp of 5 °C min^{-1}) in static air.

TiO_2-NT were treated at 550°C for 3 h (ramp of 5°C min^{-1}) in air or in ammonia (100 mL min^{-1}) to mimic the thermal polycondensation experimental condition. They are referred to as TiO_2 (*atm*), where *atm* stands for the atmosphere of the heat treatment (air or NH_3).

gC_3N_4-TiO2 nanocomposites were synthesized via a two-step process as described elsewhere.[36] First, titania NT and an equimolar amount of melamine and dicyandiamide blend were suspended in 10 mL of distilled water at room temperature (impregnation method). The solution was evaporated under vigorous stirring and the obtained powder was dried in an oven at 100 ◦C overnight. A second thermal polycondensation step was carried out in an alumina crucible with a lid at 550 °C for 3 h (ramp of 5 °C min^{-1}, flowing gas at 100 mL min^{-1}) to obtain the final composite. Nanocomposites were synthesized with a final g-C_3N_4 content ranging from 2(±0.5) wt.% to 72(±2) wt.%, as determined by thermogravimetric analysis. The g-C_3N_4 content was defined as:

$$\text{g-}C_3N_4\ (\text{wt.\%}) = m(C_3N_4)/(m(C_3N_4) + m(TiO_2))$$

The resulting materials are denoted C_3N_4(*X*%)-TiO_2 (*atm*), where *X* stands for the wt. % of C_3N_4 and *atm* stands for the atmosphere of the polycondensation treatment (air or NH_3).

Gold deposition

Au/*support* were prepared by chemical reduction of $HAuCl_4$ as gold precursor in the presence of the support.[36-38,41,42] The support (300 mg) was dispersed into a methanol/ethanol mixture (91/9 v/v, 55 mL) with a tip sonicator (700 W, 20 kHz) during 30 min, using 30% of maximum sonication power. The mixture was then transferred to a bath sonicator (280 W, 50/60Hz) and allowed to cool down to room temperature (20 °C) before the sonication was turned on. A given volume of a methanol/ethanol solution of $HAuCl_4$ (2.5(±0.2) × 10^{-3} mol L^{-1}) was then added in order to target a gold loading of 0.3 wt.%. Sonication was carried on for 1 h before 5 mL of a fresh methanol/ethanol solution of $NaBH_4$ solution (2.5 × 10^{-2} mol L^{-1}) was added. Sonication was carried on for 10 min. Finally, powders were recovered by filtration and dried at 110 °C for 12 h. The resulting materials are denoted Au/*support*, where support refers to one of the materials described above (C_3N_4 (*atm*), TiO_2 (*atm*) or C_3N_4(*X*%)-TiO_2 (*atm*)).

Characterization

Nitrogen adsorption–desorption isotherms were obtained at 77 K using a Micromeritics Asap 2420 porosimeter. Powder materials were outgassed at 250 °C under primary vacuum for 2 h prior to analysis. Specific surface areas were calculated by the Brunauer, Emmett and Teller (BET) method in the relative pressure (p/po) range 0.05–0.3 and using t-plot methods. Pore volumes and pore size distributions were calculated by the Barrett, Joyner and Halenda (BJH) method on desorption isotherms.[43]

Fourier transform infrared (FTIR) spectra were recorded by Attenuated Total Reflectance with a Thermo Fisher Nicolet iS10 spectrometer in the 525 – 4000 cm^{-1} range. Powders (few mg) are placed directly on the 2 mm × 2 mm diamond window and cover the whole surface.

Transmission Electron Microscopy (TEM) was carried out on a JEOL 2100F LaB_6 TEM/STEM microscope working at 200 kV accelerating voltage and equipped with a probe corrector for spherical aberrations, giving a point-to-point resolution of 0.21 nm. The sample is dispersed in ethanol by ultrasonication for 5 min. A drop of the solution is subsequently deposited on a copper grid covered with a holey carbon membrane for observation. Statistical Au NPs size distributions are obtained on bright field images using populations of 16-200 nanoparticles and the ImageJ software.[44]

X-ray diffraction (XRD) measurements were carried out on a D8-Advance diffractometer equipped with a LynxEye detector and operated at 40 kV and 40 mA, in a θ –2 θ mode using the Kα radiation of Cu at 1.5406 Å. The datasets are acquired in stepscan mode over the 2θ range 5–60°, using a step interval of 0.0329° and a counting time of 4 s per step. Samples are deposited on a round-shaped glass plate. Average size of titania crystalline domains is determined using the Scherrer formula from the full width at half-maximum of the main TiO_2(101) reflection at 2 θ = 25.3°.

Catalytic study

Catalytic tests are performed in a previously described[3,4,45,46] fully automated (CETRIB SARL, Andlau, France) fixed-bed flow reactor (i.d. 10 mm) loaded with 26 mg of the composites (i.e. 0.24-0.36 μmol Au in the bed). The gas mixtures balanced in He, i.e. 1% CO / 1% O2 for CO oxidation, and 24% H_2 / 1% O_2 / 1% CO for the oxidation of H2 in the presence of CO are introduced at a total flow rate of 100 mL min^{-1} (1 atm, GHSV ~ 15,000 h^{-1}). The composite is heated at 1° min^{-1} from 20 to 300 °C and then cooled down at the same rate. O_2 (and CO) conversions are determined on the basis of on-line Compact Gas Chromatograph (Interscience, Belgium) analysis, using external calibration. Selectivity to CO_2 is defined as the ratio between the number of moles of O_2 used to convert CO over the total number of moles of converted O_2. It is calculated by the ratio of half the CO conversion over the conversion of O_2. Turnover frequencies (TOF) are defined as the number of mole of CO or O_2 converted per number of mole of surface gold per second. The fraction of surface gold (gold dispersion) is determined by geometric calculations for cuboctahedral particles[47] using the average particle size measured by TEM before reaction.

Table 1. Physico-chemical characteristics of Au/C_3N_4-TiO_2 composites.

Entry	Composite support	BET surface area (m^2g^{-1})	Pore volume (cm^3g^{-1})	Au content (wt.%)[a]	Deposition yield (%)[b]	Au NPs size (nm)	Au dispersion	N° counts	CO TOF at 250°C (s^{-1})		O_2 TOF at 250°C (s^{-1})	Selectivity at 250°C (%)
									COox	PROX	PROX	PROX
0	TiO_2-380 (air)	144	1.11	-	-	-		-	-	-		
1	TiO_2-550 (air)	107	1.25	0.18	60	3.7±0.9	0.36	16	1.71	0.20	1.55	7
2	TiO_2-550 (NH_3)	103	n.a.	0.21	70	3.1±1.1	0.42	44	2.37	0.40	1.47	14
3	C_3N_4(2%)-TiO_2 (air)	64	0.69	0.19	63	3.1±0.6	0.42	27	2.79	0.35	1.44	12
4	C_3N_4(2%)-TiO_2 (NH_3)	78	n.a.	0.25	83	4.1±1.4	0.33	76	0.10	0.02	0.58	2
5	C_3N_4(75%)-TiO_2 (air)	29	0.15	0.26	87	4.2±1.7	0.32	119	0.14	0.31	1.47	11
6	C_3N_4(75%)-TiO_2 (NH_3)	33	n.a.	0.27	90	2.3±0.4	0.54	76	0.04	0.12	1.36	5
7	C_3N_4 (air)	10	0.05	0.24	81	5.1±2.4	0.27	200	0.07	0.24	2.06	6
8	C_3N_4 (NH_3)	32	n.a.	0.24	80	3.2±1.1	0.41	200	0.05	0.30	2.72	6
9	C_3N_4[26,c]	16	n.a.	0.39	n.a.	2.8±0.9	0.49	497	0	n.a.	n.a.	n.a.
10	SiO_2[6,d]	220	n.a.	1.8	n.a.	30	0.05	n.a.	0.04	n.a.	n.a.	n.a.
11	TiO_2[6,e]	40	n.a.	2.4	n.a.	2.9	0.46	n.a.	1.3	n.a.	n.a.	n.a.

[a] Determined by ICP measurements

[b] Defined as the ratio between the real Au content as measured by ICP and the targeted Au content (0.3 wt.%) derived from the amount of gold used in the synthesis

[c] P_{O_2} = 6 kPa, GHSV = 5000 h^{-1}

[d] P_{CO} = 4.9 kPa, P_{O_2} = 4.8 kPa, T = 80°C, GHSV = 3330 h^{-1}

[e] P_{O_2} = 20 kPa, T = 80°C

RESULTS AND DISCUSSION

Morphology of C_3N_4-TiO_2 composites (Nitrogen physisorption).

Full nitrogen physisorption isotherms were recorded on TiO_2 and C_3N_4 references, as well as on the low and highly loaded C_3N_4-TiO_2 composites obtained in air (Figure 1a) and in ammonia (Figure 1c).

After synthesis, titania nanotubes exhibit a Type IV isotherm, according to the IUPAC nomenclature, with a H3 hysteresis which corresponds to mesoporous materials.[43] The mesoporosity originates from the intertube void, as

well as the open space inside the tube. The pore size distribution (Figure 1c) exhibits two maxima at 7 nm and 20 nm. The lower pore size is consistent with the inner tube diameter determined by TEM (Figure S1). The larger pore size is attributed to the empty space created by the aggregation of nanotubes. It is consistent with the dimensions of the tubes (outer diameter of 15 nm, length of about 130 nm) and TEM observations. The measured BET surface area of 144 m^2g^{-1} (Table 1) is also quite close to the calculated geometric surface of tubes of those dimensions (128 m^2g^{-1}).

After further calcination at 550°C, the overall surface area decreases by about 30% (to 105±2 m^2g^{-1}), regardless of the atmosphere of calcination (Table 1), due to partial collapse and sintering of the tubes (Figure S1). The population of smaller pores is decreased and shifted to larger sizes, with maxima at 10 nm (Figure 1c,d), but the pore volume remains similar.

Unlike titania, air-derived C_3N_4 exhibits a type II isotherm (Figure 1a), i.e. a reversible isotherm with virtually no hysteresis typical of non-porous materials,[43,48] and a low surface area of 10 m^2g^{-1} (Table 1). Virtually no mesoporous volume (0.05 cm^3g^{-1}, Table 1) is created when C_3N_4 is produced in air, in accordance with previous results.[38] This indicates a highly packed and compact structure.[49]

Morphology of the C_3N_4-rich composite grown in air is similar to that of bare C_3N_4. Nevertheless, the composite appears a little more porous. It exhibits a Type IV isotherm with a H3 hysteresis loop (Figure 1a). The pore volume and the surface area are about three times higher than those found for raw C_3N_4 (Table 1), which shows that titania acts as a dispersing agent for C_3N_4. The maximum at 7 nm in the pore size distribution (Figure 1c) suggests that the porosity of the composite may correspond to the inner volume of the incorporated titania tubes. The intensity of the peak, which is decreased by about 75% in the C_3N_4(75%)-TiO_2 composite, as compared with pure titania NT (heated at 550°C, i.e. at the same temperature than that used in the polycondensation process), is consistent with this model. Further, the absence of larger pores, as those found in pure titania NTs agglomerates, suggests that C_3N_4 fills the intertube space in the composite.

Morphology of the low loaded C_3N_4-titania composite resembles more that of titania. Nevertheless, surface area ad pore volume are about 40% lower. The absence of the peak at 7 nm in the pore size distribution (Figure 1c) suggests that the C_3N_4 has polycondensed within titania NTs, filling the inner space. It is interesting that the outer volume also decreases, by about 50% as compared with pure titania NT, despite the very low C_3N_4 loading of 2wt.%. Besides, high resolution TEM images show coverage of titania by very thin layers of C_3N_4 (Figure 2b-c). This is attributed to a molecular interaction between C_3N_4 precursors and/or their gaseous decomposition products (NH_3, HCN, cyanuric acid, isocyanate)[50] and the hydrophilic, OH-terminated TiO_2 surface.[51,52] We speculate that the polycondensation process is then directed by the titania surface,[53] which drives/controls the morphology of the resulting composites, and that C_3N_4 acts as a glue that makes the titania NTs agglomerated structure more compact.

When grown in ammonia, raw C_3N4 exhibits a Type IV isotherm with a H3 hysteresis (Figure 1b). The surface area is three times higher than that of the raw air-derived carbon nitride (Table 1), in accordance with previous results.[38] More importantly, the porous volume is one order of magnitude higher with a much larger pore size distribution centered at about 40 nm (Figure 1d). Such a large mesoporous volume is indicative of the loose packing of extended C_3N_4 layers.[49] It is consistent with the high "crystallinity" of ammonia-derived C_3N_4, i.e. the growth of 2D layers instead of the 1D linear melon and dimelem structures produced upon polymerization in air, as shown by a previous XRD study.[38]

Morphology of the C_3N_4-rich composite grown in ammonia is similar. It is characterized by a similar surface and an only slightly lower pore volume (Table 1). The pore size distribution exhibits two local maxima, one at 10 nm and one at 40 nm (Figure 1d). The first one is attributed to the inner porosity of the incorporated titania tubes. The second one is attributed to mesoporosity of C_3N_4. The slightly lower intensity of this larger pore size is consistent with partial filling of the C_3N_4 mesoporosity by titania, which is supported by the observation of embedded titania NTs on TEM images (Figure 3c, d). Yet, the large pore size remains the most significant feature of the porosity of this composite.

Morphology of the low loaded ammonia-derived C_3N_4-titania composite is peculiar. Its surface area is similar to that of its air-derived counterpart (Table 1). However the pore size distribution obtained in ammonia significantly differs from all other size distribution patterns (Figure 1d). It consists in small mesopores ranging from 2 to 30 nm with local maxima at 9 nm, 14 nm and 21 nm. The intensity of this event is much larger than the one that could be expected from the inner tube porosity of titania. It has been observed before upon splitting of C_3N_4 sheets, i.e. decrease in the C_3N_4 2D layers dimensions.[49] It suggests that, at high concentration, TiO_2-NTs act as inhibitors of the ammonia-driven growth of C_3N_4 planes. At the same time, the large mesoporosity observed for titania NTs aggregates is markedly reduced. It suggests that the intertube void is largely filled by C_3N_4. The partial filling of the pores (i.e. not just increase in the percolation state of the structure, like in the air-derived counterpart) also creates a smaller porosity, which contributes to the peculiar porous profile observed (Figure 1d). Given the low amount of C_3N_4 present in the composite, a reasonable model that could fit these observations is the growth of stacks of very small C_3N_4 sheets normal to the tubes. Hence, the titania-inhibited 2D structures of C_3N_4 obtained in ammonia exhibit the narrowest pore size distribution with the lowest average pore size.

In summary:

- At high C_3N_4 loadings, the morphology and porosity of C_3N_4-TiO_2 composites is essentially dominated by C_3N_4

features, i.e. the growth of porous stacks of extended 2D sheets in ammonia (large pores) and the growth of a more compact, intricate structure composed of entangled less perfect 2D sheets and 1D chains in air (poorly porous), as illustrated by TEM images (Figure 3). The presence of titania thus barely affects the growth of C_3N_4. Titania creates some small porosity in the air-derived composite and occupies part of the large mesoporosity in the ammonia-derived composite.

- At low C_3N_4 loadings, the growth of C_3N_4 seems driven by both the polycondensation atmosphere and titania, somehow acting as hard template.[54,55] TEM images of such low loaded C_3N_4-TiO_2 composites are clearly dominated by quite similar titania aggregates with more (ammonia, Figure 2e,f) or less (air, Figure 2c,d) filled intercrystallite porosity, associated with markedly different pore size distributions. While the air-derived composite exhibits a pore size distribution (at larger pore sizes) similar to that of C_3N_4-free, pure titania, the ammonia-derived composite exhibits smaller pores than both its titania and C_3N_4 counterparts. Hence, under constrained conditions (low ratio of C_3N_4 precursors vs. TiO_2), filling of the titania intertube void by C_3N_4 is critically dependant on the polycondensation atmosphere. The porous profiles of low loaded C_3N_4-TiO_2 composites suggest that air drives the growth of C_3N_4 alongside titania structures (filling the inner void and covering the outer surface without filling the external volume), while ammonia drives the growth of C_3N_4 composites normal (or at least with a much higher angle relative) to the titania surface (partially filling the external porosity, which decreases the average pore size).

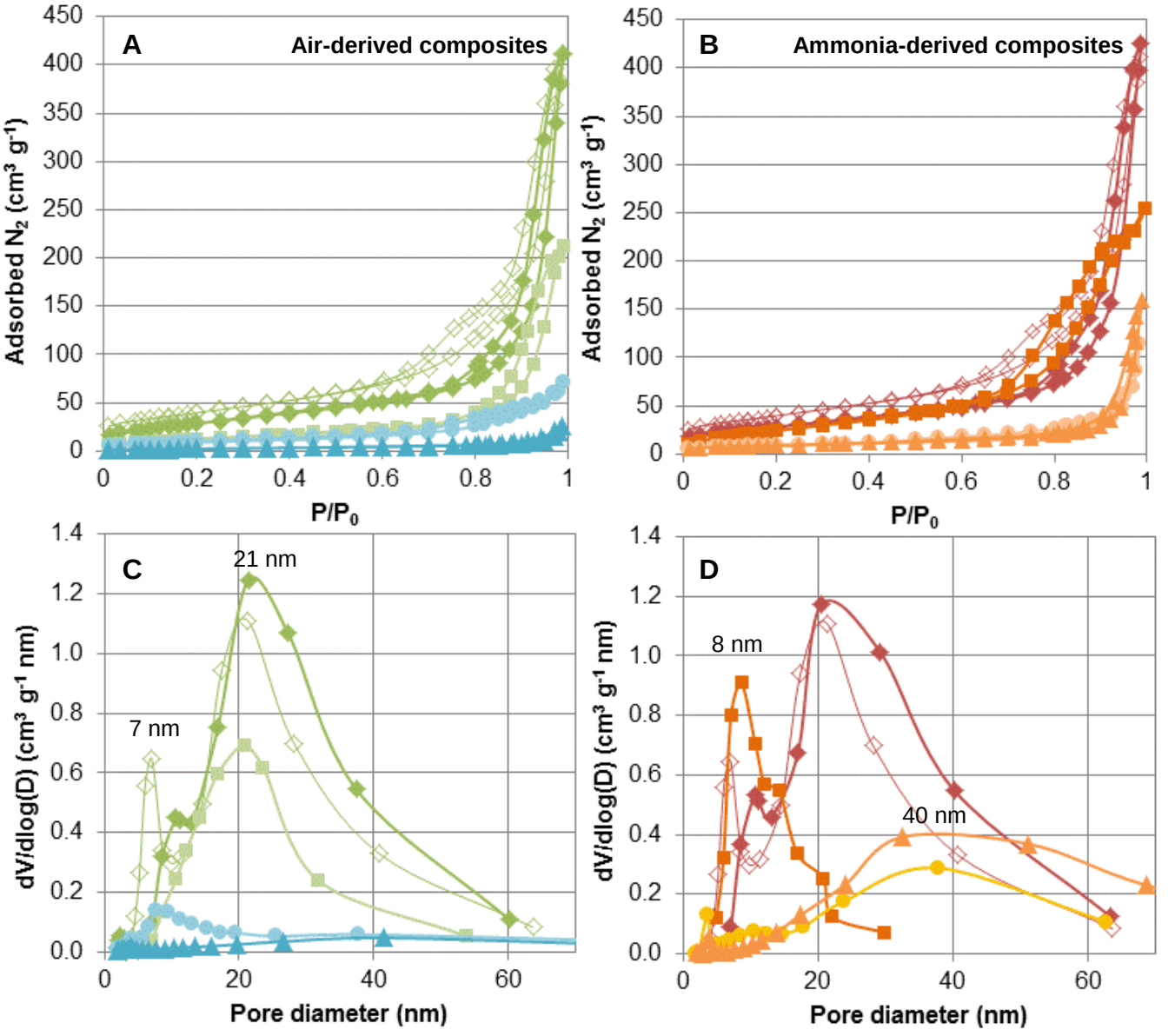

Figure 1. Texture and porosity of C_3N_4-TiO_2 composites. N2 physisorption isotherms (a, b) and pore size distributions (c, d) of the composites prepared in air (a, c) and in ammonia (b, d). C_3N_4 (▲), C_3N_4(75%)-TiO_2 (●), C_3N_4(2%)-TiO_2 (■), TiO_2-550 (◆), TiO2-380 (◇).

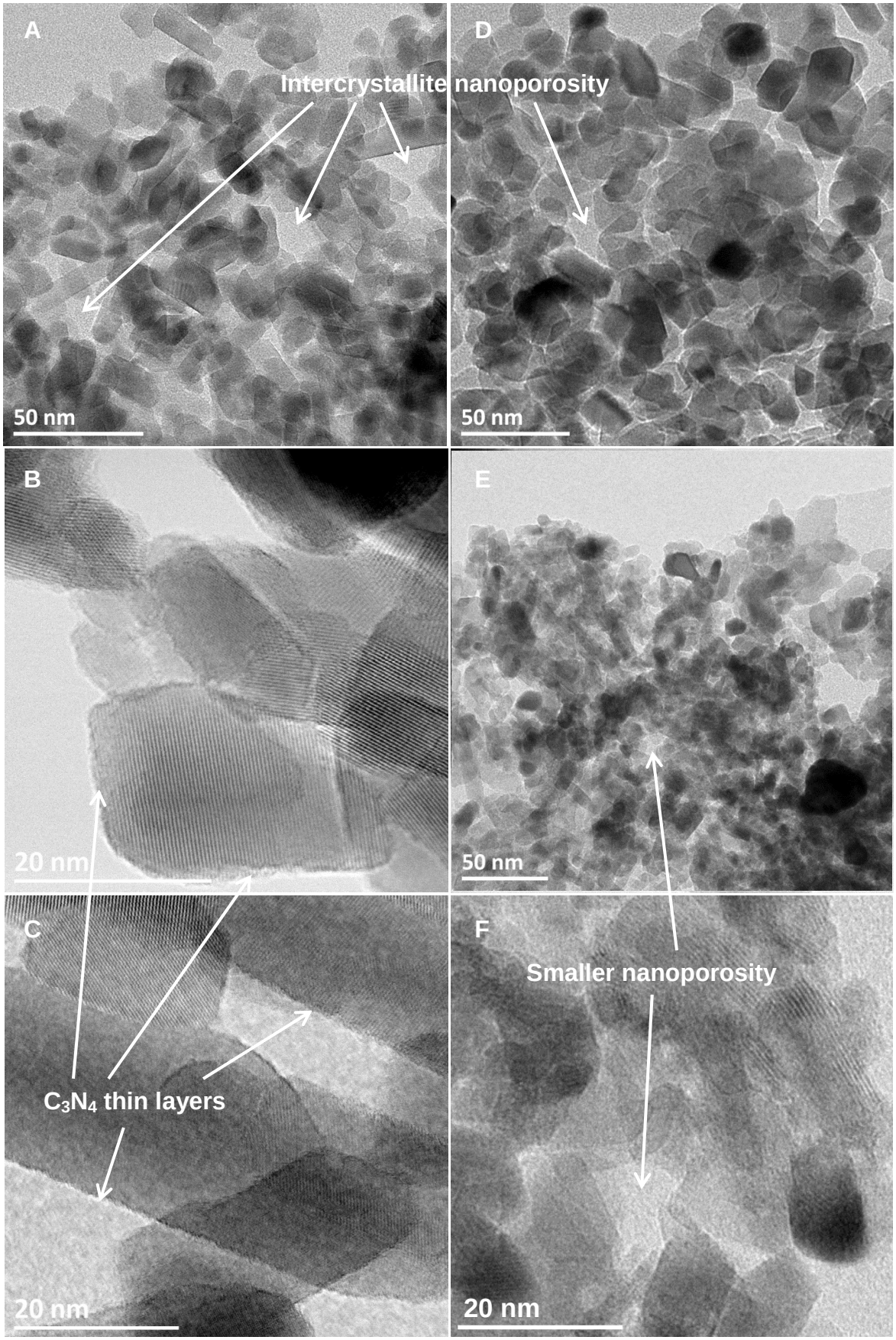

Figure 2. Morphology of low loaded C_3N_4-TiO_2 composites. TEM images of air-derived TiO2-550 (A), air-derived C_3N_4(2%)-TiO_2 (B-D) and ammonia-derived C_3N_4(2%)-TiO_2 (E, F).

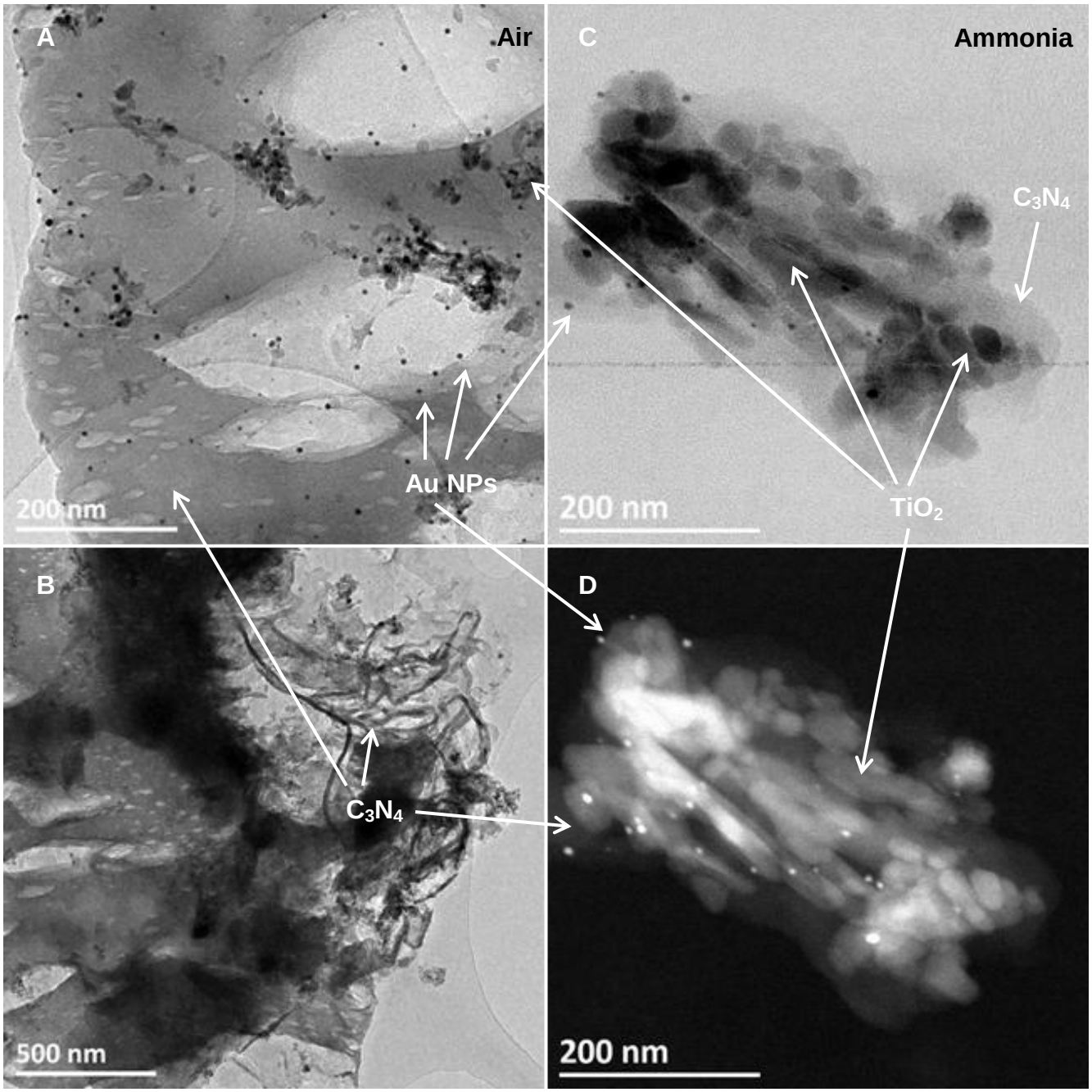

Figure 3. Morphology of highly loaded C_3N_4-TiO_2 composites. TEM images of air-derived (A, B) and ammonia-derived (C, D) Au/C_3N_4(75%)-TiO_2 composites.

Interaction between C3N4 and titania and surface composition. ATR FTIR was used to characterize both bulk and surface vibrations of the materials, which allows to further understand how titania and carbon nitride interact at the nanoscale, and further support the presence of C_3N_4 on the titania surface in the low loaded composites. Titania and carbon nitride are characterized by different vibration patterns. Full range FTIR spectra of titania nanotubes are characterized by 3 major absorption regions, regardless of the treatment, air or ammonia, they are submitted to (Figure 4 a,b, green and brown - - - lines). The broadest and most intense absorption feature between 400 and 1000 cm^{-1} corresponds to Ti-O-Ti and Ti-O stretching vibrations from the titania framework. The large absorption band at 3360 cm^{-1} corresponds to stretching vibrations of H-bonded terminal hydroxyl groups and physisorbed water, while the smaller feature at 1630 cm^{-1} corresponds to the bending vibrations of adsorbed water. Full range FTIR spectra of carbon nitrides are characterized by 2 major absorption regions, regardless of the atmosphere, air or ammonia, they have been synthesized in (Figure 4 a, b, blue and orange ··· lines). The most prominent multi-peak feature between 750 and 1750 cm^{-1} (Figure 4 d, f) corresponds to skeletal and in-plane vibrations

of polyaromatic units, namely C=N skeletal stretching modes of heterocycles at 1623 cm^{-1}, to side-chain asymmetric C-N stretching vibrations at 1534 and 1561 cm^{-1}, to C-N skeletal stretching modes of aromatic rings at 1456, 1397 and 1312 cm^{-1}, to C-NH-C bridges *via* NH linear linkage of heptazine units at 1227 and 1201 cm^{-1} and to the breathing mode of triazine units at 803 cm^{-1}.[57] On the other hand, the broad band centered at about 3150 cm-1 is composed of 3 components at 3080, 3160 and 3260 cm^{-1}, due to vibrations of out of plane terminal NH and $-NH_2$ functions (uncondensed amine groups) and physisorbed water (Figure 4 c, e), which are characteristic of the C_3N_4 outer surface.

Interestingly, the vibration pattern of titania is significantly modified in the low loaded composite. Comparing the green dotted - - - and plain lines in Figure 4a or the brown dotted - - - and plain lines in Figure 4b, it appears that the addition of only a minor amount of C_3N_4 to TiO_2 NTs induces major inhibition of both the terminal and framework vibrations of TiO_2 NTs. The band related to terminal hydroxyl groups (3360 cm^{-1}) and the bands related to bulk Ti-O stretching vibrations (400-1000 cm^{-1}) indeed all markedly decrease. On the other hand, skeletal and terminal vibrations characteristic of the C_3N_4 framework appear quite clearly between 1200 and 1650 cm^{-1} and at 3150 cm^{-1}, respectively. The fact that titania vibrations are inhibited in this composite suggests extensive coverage of the titania surface by C_3N_4, in agreement with N_2 physisorption results (Figure 1), and strong interaction between C_3N_4 and TiO_2.[58] When the C_3N_4 content is further increased to 72 wt.%, the FTIR spectrum becomes very similar to that of pure C_3N_4 (compare - · - · - · – and ··· lines) regardless of the polycondensation atmosphere (air or ammonia). This shows that the polycondensation of C_3N_4 precursors on top of titania nanotubes drastically modifies the surface chemical composition of titania and that the surface chemistry of all composites is dominated and controlled by C_3N_4.

On the other hand, concerning the effect of the atmosphere, one can notice that the atmosphere of the post-synthesis treatment of titania NTs apparently does not affect the surface chemistry of titania as the water-normalized IR spectra of ammonia- and air-treated titania NTs are quasi-identical (Figures 4 c, d, - - - lines). However, the polycondensation atmosphere that is used for C_3N_4 synthesis has a subtle impact on the surface chemistry of C_3N_4 (Figure 4 e, f, ··· lines). In particular, NH_3-derived C_3N4 exhibits a more prominent feature at 3150 cm^{-1} than air-derived C_3N_4, associated with decreased vibrations at 1201 and 1227 cm^{-1}. This indicates that the NH_3-derived carbon nitride is much more functionalized with out of plane NH and NH_2 functions and that the occurrence of linear linkages of heptazine units, such as dimelem and melon, is significantly lower than in the air-derived composite. It is consistent with our previous XRD study of C_3N_4 which showed that the air-derived materials is more linear (1D), while the NH_3-derived material is more crystallized (3D stacking of large planes).[38] It is interesting that these differences in the functionalization and morphology of C_3N_4 are retained in the low loaded C_3N_4-TiO_2 composites (Figures 4 c, d, plain lines) and that the NH_3-derived material is the only composite that exhibits a distinct vibration band at 2040 cm^{-1} corresponding to the =C=N- stretching vibration of ketinimine derivatives (R2C=C=N-R).[59-62] On the contrary, in the C_3N_4-rich composites, the presence of titania masks differences in functionalization of the C_3N_4 component obtained under different polycondensation atmospheres. No significant difference is indeed observed in the FTIR spectra of highly loaded C_3N_4-TiO_2 composites (Figures 4 e, f, - · - · - · – lines). This means that similar free terminal groups are present on the two quite different C_3N_4 morphologies (Figure 1c, d, Figure 3). This suggests that carbon nitride strongly interacts with the titania surface, possibly via the functions corresponding to the diminished vibrations, blocking these vibrations upon immobilization.

Gold deposition.

Gold was deposited onto C_3N_4, TiO_2 and C_3N_4-TiO_2 composites using a sonicated-assisted chemical reduction method performed in the presence of the support. Deposition yields of 60 to 90% are achieved (Table 1). They are minimal over pure titania NTs despite their larger surface areas (60-70%), indicating a poorer affinity of the titania surface for chloroauric anions and gold nanoparticles, as compared with the C_3N_4 surface (80%). They are higher (83-90%) on all C_3N_4-TiO_2 composites, except C_3N_4(2%)-TiO_2 (air), and maximal for the C_3N_4(75%)-TiO_2 composition. The similarities in deposition yields for 3 out of the 4 composites (entries 4-6) are attributed to their similar surface chemistries, as shown by FTIR.

Average Au NPs sizes have been statistically determined by measuring their diameters on TEM images. Although they are obtained on differently-sized populations (due to lower contrast, associated with lower loading, of the titania-rich samples), they are found representative of the population of each composite. They essentially vary between 3.1 and 4.2 nm (Table 1). A lower average size (2.3 nm) is found for the NH_3-derived C_3N_4-rich composite, suggesting a particularly strong affinity between gold precursors and the support surface. The larger size (5.1 nm) found for air-derived pure C_3N_4 is attributed to the particularly low surface area and porous volume of the composite support (10 $m^2\ g^{-1}$ and 0.05 $cm^3\ g^{-1}$, the lowest of the series).

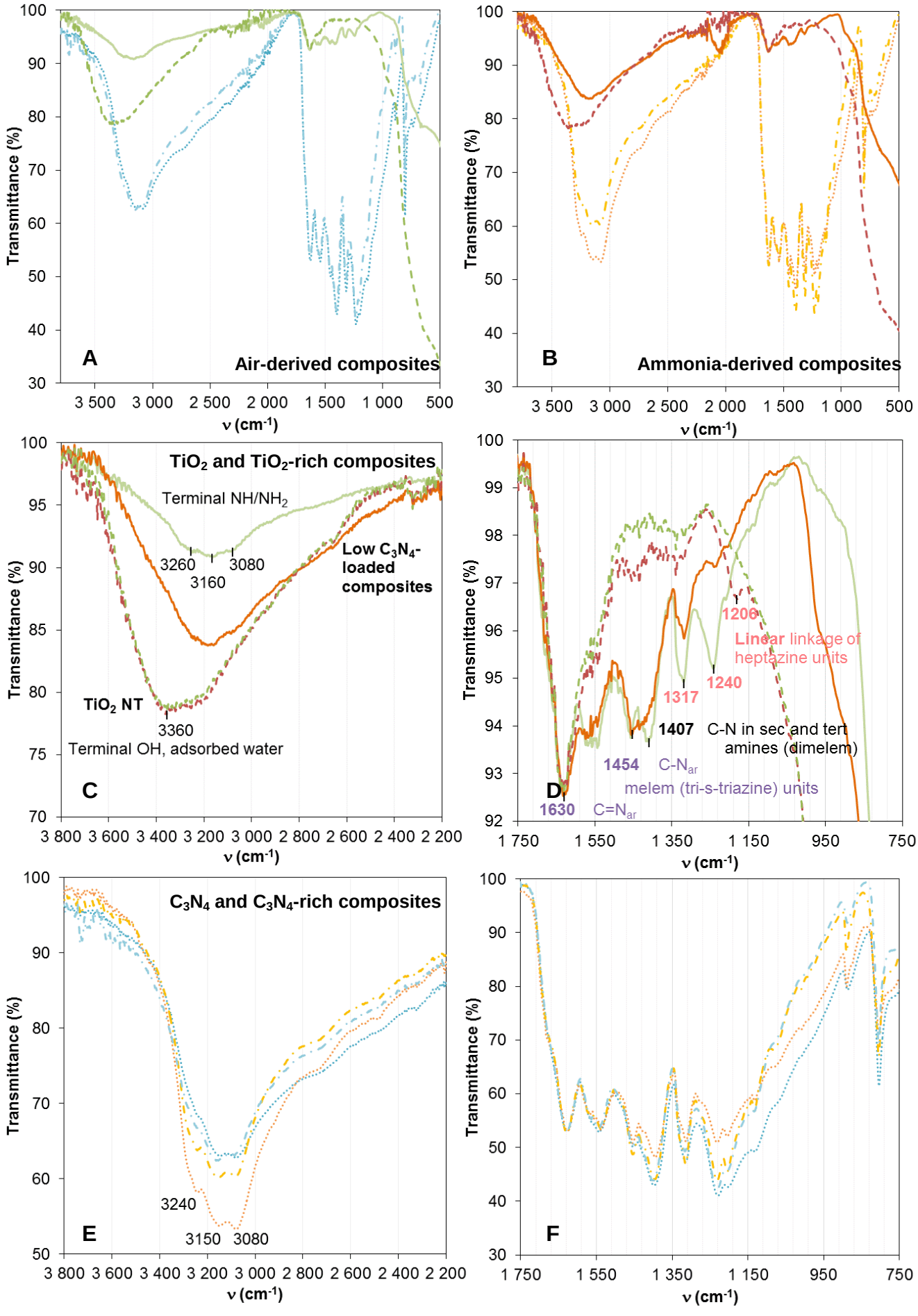
A
Air-derived composites
Transmittance (%)
ν (cm-1)
B
Ammonia-derived composites
C
TiO2 and TiO2-rich composites
Terminal NH/NH2
3260
3160
3080
Low C3N4-loaded composites
TiO2 NT
3360
Terminal OH, adsorbed water
D
1206
Linear linkage of heptazine units
1240
1317
1407
C-N in sec and tert amines (dimelem)
1454
C-Nar
melem (tri-s-triazine) units
1630
C=Nar
E
C3N4 and C3N4-rich composites
3240
3150
3080
F

Figure 4. Surface chemical composition of C_3N_4-TiO_2 composites. Full range FTIR spectra of the air (a) and ammonia (b) series. 2200-3800 cm^{-1} (c) and 750-1750 cm^{-1} (d) regions of FTIR spectra of TiO_2 NT and low C_3N_4-loaded composites normalized against the 1630 cm^{-1} vibration corresponding to adsorbed water. 2200-3800 cm^{-1} (e) and 750-1750 cm^{-1} (f) regions of FTIR spectra of C_3N_4 and C_3N_4-rich composites normalized against the 1623 cm^{-1} vibration, corresponding to C=N skeletal stretching modes of aromatic rings.[56] C_3N_4 (blue and orange · · ·), C_3N_4(75%)-TiO_2 (blue and yellow - · - · - · -), C_3N_4(2%)-TiO_2 (plain lines), TiO_2-550 (green and brown - - -).

CO oxidation catalysis.

The gold-catalyzed CO oxidation reaction is a very useful reaction, as it is size- and support- dependent. This has been demonstrated in details by a huge amount of studies in the last three decades.[63] Based on this intensive work, and provided Au NPs are "catalytically sized" and with similar sizes, variations in the intrinsic reaction rate can teach a lot on the accessibility of Au NPs and on the surface composition of the support. CO and O_2 TOFs, as well as selectivities, at 250°C are shown in Table 1 and Figure S2. Light-off curves are shown in Figure 5. The high light-off temperatures observed over our materials (~ 200°C) compared to state-of-the-art catalysts (20°C) are due to the high GHSV, low Au content of the catalytic bed and low partial pressure of oxygen used in this study.

H_2-free CO oxidation

Looking at Figure 5 (a, b), one can see that the least performing composites are C_3N_4 and C_3N_4-rich materials, regardless of the atmosphere in which they are synthesized (air or ammonia). Effects related to gold particle size can be ruled out, due to the similarity with values obtained for the other materials. These materials have been shown to mainly expose the C_3N_4 surface (see FTIR, N_2 physisorption, TEM). It means that C_3N_4 is an "inert" support for gold using the terminology defined by Schubert *et al.*.[6] This is in agreement with the work by Veith *et al.*.[26] It is explained by the absence of functions capable of activating oxygen (bulk oxygen, oxygen vacancies and hydroxyl groups).

For the ammonia-derived series (Figure 5b), the best performing catalyst is Au/TiO_2, a reference for CO oxidation due to the suitable surface chemistry of titania[8-11] towards oxygen activation.[13,14] The deposition of only a minor amount of C_3N_4 (2wt.%), prior deposition of gold, drastically inhibits CO conversion. This supports the full coverage of TiO2 external surface by C_3N_4 suggested by N_2 physisorption and IR characterizations. Indeed, surface chemistry of the composite was shown to be dominated by the C_3N_4 IR signature (Figure 4 b, c), with disappearance of titania terminal functions. This composite is also characterized by the presence of ketinimine and by the loss of the inter-TiO_2 crystallites volume (Figure 2d), which could result in full deactivation of the titania surface.[64]

On the other hand, for the air-derived series (Figure 5a), the low loaded Au/C_3N_4(2%)-TiO_2 composite surpasses Au/TiO_2. This can be related to the peculiar morphology of the composite support. First, it means that carbon nitride and titania are mixed in such a way that titania-mediated oxygen activation pathways are still active, despite partial coverage of the titania nanostructures with C_3N_4 evidenced by IR (Figure 4 a, c, d) and N_2 physisorption (Figure 1a) experiments, and in particular despite loss of terminal OH groups, highlighting the occurrence of alternative support oxygen-driven pathways.[10,11] Second, it means that Au NPs are more accessible, due to the higher compacity of the support and in particular loss of the small mesoporosity (Figure 1c). Gold-catalyzed CO oxidation is indeed slower when gold nanoparticles are confined within small mesopores supports, due to internal diffusion limitations.[65]

PROX

Overall variations of CO TOF with C_3N_4 content of the support are drastically limited by the presence of excess hydrogen in the feed (H_2/CO = 24) (Figure 5c, d, Figure S2, Table 1). This is attributed to two phenomena. On one hand, the titania-rich catalysts are inhibited by the presence of hydrogen for both the air-derived (Figure 5c) and ammonia-derived (Figure 5d) series. On the other hand, C_3N_4-rich catalysts are promoted by the presence of hydrogen (increased CO TOF). Indeed, considering CO TOF at 250°C (Table 1, Figure S2), the intrinsic activities of air-derived Au/TiO_2 and Au/C_3N_4(2%)-TiO_2 are decreased by a 8-fold, while the activities of air-derived Au/C_3N_4 and Au/C_3N_4(75%)-TiO_2 are enhanced by a three-fold and a two-fold, respectively. As a result, the two air-derived references Au/TiO_2 and Au/C_3N_4 perform quite similarly throughout the temperature range considered (Figure 5c, Figure S2), despite the huge differences in support surface areas, porosities and surface functionalities. It means that the surface chemistry of the support no longer impacts the performance of gold for CO oxidation at these temperatures, where the oxidation of hydrogen dominates (selectivity to CO_2 essentially below 15%, Figure S2).[66] Hence, over these materials, the oxidation of CO under PROX conditions is attributed to the occurrence of support-independent, H_2-mediated[17] or H_2O-mediated[16, 22] oxygen activation pathways. It shows for the first time, that these specific oxygen activation pathways are possible on NH_2-terminated support surfaces, i.e. that they do not require the support surface to be hydroxylated.

Comparison of the overall oxidation activity of the composites under PROX conditions (oxygen TOF, Figure 5 e, f) confirms that the performance is no longer a function of the surface chemistry of the support and shows that it is impacted by the porosity of the support instead. On one hand, performances of air-derived composites are similar throughout the temperature range considered (Figure 5e), with O_2 TOF at 250°C ranging from 1.44 to 2.06 s^{-1} whatever the C_3N_4 content of the support (Table 1, Figure S2), despite the large differences in surface chemistries and in H_2-free CO oxidation performances (Figure

5a, Figure S2). On the other hand, performances of the ammonia series are much more dependent on the C_3N_4 content (Figure 5f), with O_2 TOF at 250°C ranging from 0.58 to 2.72 s^{-1} (Table 1, Figure S2), and apparently controlled by the *porosity* of the support. Indeed, the catalyst with a higher average pore size (40 nm) than the titania-supported catalyst (21 nm), i.e. the C_3N_4–supported catalyst, performs better, while the catalyst with a lower average pore size (8 nm), namely the titania-rich composite, performs worse. The C_3N_4-rich composite performs similarly to Au/TiO_2-550 (NH_3) due to the presence of smaller pores (8 nm), in addition to the larger pores (40 nm), which may confine part of gold nanoparticles and limit their access, so that not all the catalytic surface is easily available.

By comparison, the air series (Figure 5e) performs similarly to the ammonia-derived TiO_2-supported catalyst (Figure 5f, Figure S2). Hence, titania-based catalysts, with similar pore size distributions whether treated in air or in ammonia, perform similarly. The air-derived titania-rich composite shows a similar activity as well, and similar average pore size (21 nm). It markedly contrasts with its ammonia counterpart, which exhibits the lowest activity of all and also the smallest average pore size. Finally, for the C_3N_4 and C_3N_4-rich catalysts, a smaller difference in activities is found between the two series. The ammonia-derived C_3N_4 catalyst, which shows the largest average pore sizes (40 nm) and the absence of any small pores, performs only slightly better than its essentially non-porous air-derived counterpart.

Hence, the impact of the porosity on the overall catalytic oxidation performance of these Au/C_3N_4-TiO_2 composites in PROX can be described in terms of ease of oxygen diffusion towards the catalytic gold nanoparticles. The most active catalyst is that with the largest pores (40 nm) and no small pores, closely followed by those with no pores in which the slightly less dispersed Au NPs are located on the outer surface and thus easily accessible. The least active catalyst is the one with the lowest average pore size, which contains no large pores.

Hence, the ammonia-derived C_3N_4 gold catalyst, which is inactive for CO oxidation due to the inadequate support surface chemistry (Figure 5b), exhibits the highest overall PROX activity amongst all supports studied here (Figure 5f, Figure S2), due to its large pore size distribution ranging from 10 to 90 nm. This is much larger than the size of the reactant and product molecules involved in the process (CO, O_2, CO_2, H_2, H_2O). The need for a pore size >> 10 nm suggests that cumbersome molecular intermediates may be involved in gold-catalyzed PROX over inert supports, i.e. that intermediates larger than the usually postulated OOH-type species[16,17] may be needed to activate oxygen *via* hydrogen- and water-mediated pathways.

The selectivity of the PROX reaction at 250°C (Table 1, Figure S2) is quite low for all the catalysts, i.e. below 15%. It is attributed to the high light-off temperatures for CO oxidation, which makes it detectable in a temperature range where hydrogen oxidation severely competes.[66,67] Nevertheless, it is interesting that the selectivity of the PROX reaction varies with the C_3N_4 content of the support in a similar manner as that observed for CO TOF, with a stronger dependence however on the C_3N_4 content (Figure S2). The ammonia series contains the most selective (Au/TiO_2, 14%) and least selective (Au/C_3N_4(2%)-TiO_2, 2%) catalysts. Hence introducing only 2% of C_3N_4 on the titania support prior to gold deposition drastically lowers the selectivity of the catalyst. This could be attributed to the drastic reduction in pore size from 20 to 8 nm, which likely has more impact on the oxidation of CO than on the oxidation of the smaller, labile hydrogen molecule. The C_3N_4-rich and C_3N_4 materials with larger pores exhibit a little higher selectivities of 5 and 6%, respectively. Hence, for the ammonia series, the selectivities of the composites are lower than the selectivities of the single components. On the contrary, for the air series, the growth of C_3N_4 over titania NTs is beneficial to the selectivity, which reaches 12% over C_3N_4(2%)-TiO_2 and 11% over C_3N_4(75%)-TiO_2 vs. 6-7% for the single components. This synergy can be attributed to partial masking of unselective sites of the titania surface, i.e. OH groups which, under PROX conditions have been shown to promote hydrogen oxidation.[17,23] All in all, air-derived composites are significantly more selective (11-12%) than their ammonia counter-parts (2-5%), which highlights the more suitable interfacing between titania and carbon nitride obtained by polycondensation of C_3N_4 precursors in air for the PROX reaction.

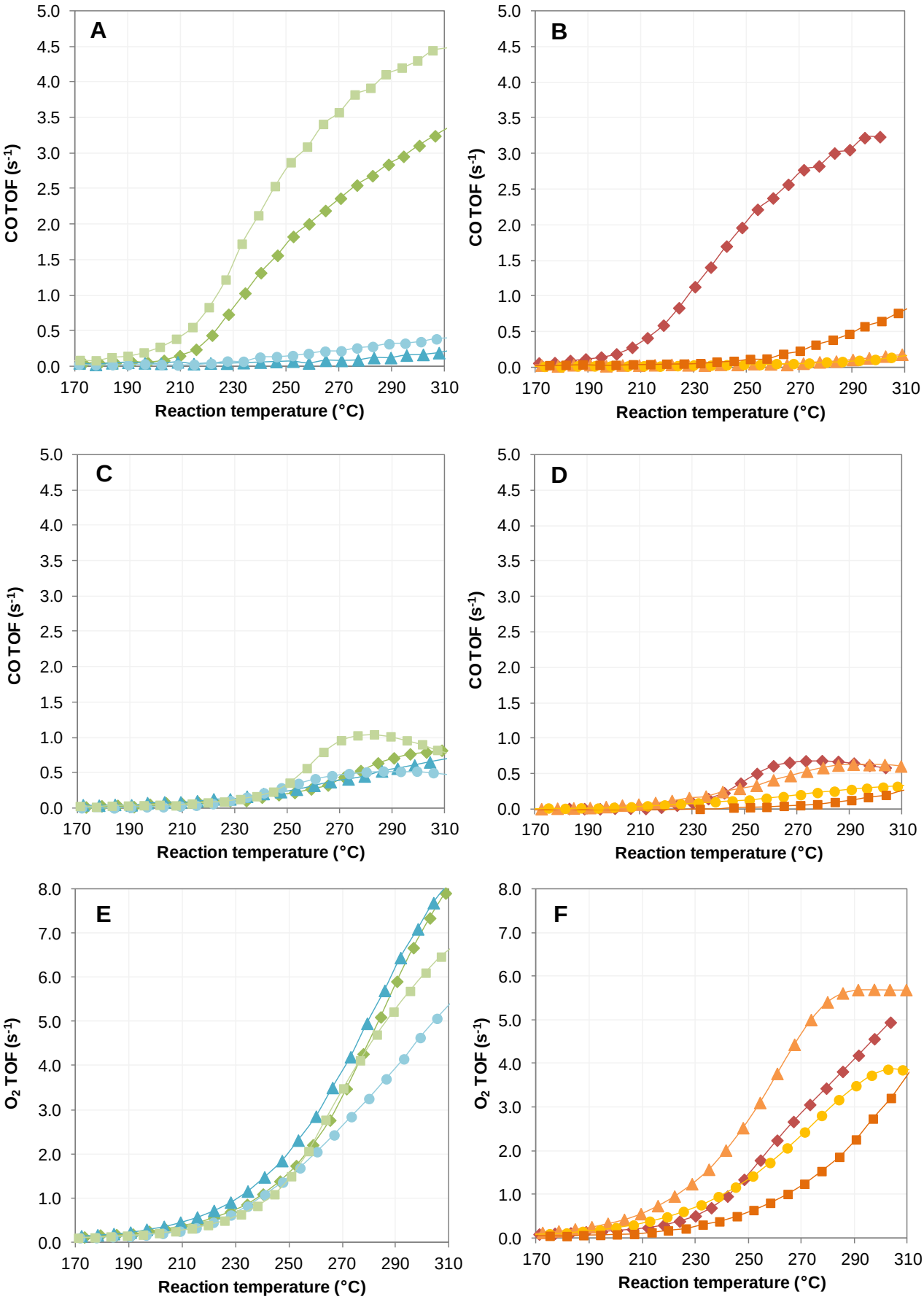
A
B
C
D
E
F
CO TOF (s-1)
O2 TOF (s-1)
Reaction temperature (°C)
0.0
0.5
1.0
1.5
2.0
2.5
3.0
3.5
4.0
4.5
5.0
6.0
7.0
8.0
170
190
210
230
250
270
290
310

Figure 5. Catalytic properties of Au/C_3N_4-TiO_2 composites. CO conversions obtained in the CO oxidation (a, b) and PROX (c, d) reaction over composites of the air (a, c) and ammonia (b, d) series. Oxygen conversions in PROX (e, f). C_3N_4 (▲), C_3N_4(75%)-TiO_2 (●), C_3N_4(2%)-TiO_2 (■), TiO_2-550 (◆).

CONCLUSION

Successful control of the surface chemistry and mesoporosity of C_3N_4-TiO_2 composites was achieved at low C_3N_4 contents by tuning the growth of C_3N_4 over pre-formed anatase titania nanotubes with two different polycondensation atmospheres (air and ammonia). Air hardly affects the mesoporosity of the intertube space (centered at 20 nm and extending over 55 nm), due to the growth of thin C_3N_4 layers partially covering titania crystallites surface. On the contrary, a quite narrow size distribution of small pores centered at 8 nm is created under ammonia, due to partial filling of the intertube space by short, stacked C_3N_4 layers. After deposition of similarly sized Au NPs on the composites, it is found that:

(1) gold-catalyzed CO oxidation is critically dependent on the surface chemistry of the mixed support and requires the presence of oxygenated surface functions

(2) the presence of only a small amount of uncovered titania surface is enough to warrant oxygen activation and activity in CO oxidation

(3) Au/C_3N_4 is active for PROX, i.e. hydrogen/water-mediated CO oxidation pathways are active on otherwise "inert" non-hydroxylated, NH_2-terminated C_3N_4 supports

(4) activity in PROX is controlled by the porosity of these intricate composite supports, regardless of their surface chemistry, i.e. by the diffusion of activated oxygen species towards the confined Au NPs; large pores (40 nm) are needed, suggesting that rather large multi-molecule intermediate scaffolds are involved

(5) selectivity in PROX, although low, benefits from the favorable interfacing between C_3N_4 and TiO_2 obtained by polycondensation in air

(6) modification of titania by a low amount of C_3N_4 (2wt.%) leads to the best catalytic performances

This study highlights the often overlooked pore size domain that should be targeted when designing gold PROX catalysts and, more generally, the relevance of compositions at the very edge of the range for binary composites.

ASSOCIATED CONTENT

Supporting information

Characterization of morphology and stability of titania nanotubes (TEM, XRD) and additional catalytic graphs.

AUTHOR INFORMATION

Corresponding Author

* E-mail: caps@unistra.fr

Present address

† Max Planck Institute of Colloids and Interfaces, Department of Colloid Chemistry, Potsdam, 14476, Germany.

ORCID

Pablo Jiménez-Calvo: 0000-0002-9826-6995

Valérie Keller: 0000-0002-3381-1446

Valérie Caps: 0000-0001-9330-2566

Author Contributions

The manuscript was written through contributions of all authors.

Funding Sources

French National Research Agency (OH-Risque Program, PICATA project, ANR-14-OHRI-0005-01).
University of Strasbourg (IdEx Program, Dr-Ing. Pablo Jiménez-Calvo Ph.D. fellowship).

Notes

The authors declare no competing financial interest.

ACKNOWLEDGMENT

The French National Research Agency (OH-risque Program, PICATA project, ANR-14-OHRI-0005-01) and the University of Strasbourg (IdEx Program, Dr-Ing. Pablo Jiménez-Calvo Ph.D. fellowship) are thanked for funding. F. Vigneron (ICPEES, CNRS UMR 7515) is thanked for technical support on nitrogen physisorption studies. D. Ihiawakrim (IPCMS, UMR 7504) is thanked for acquiring TEM images.

ABBREVIATIONS

NPs, nanoparticles; NTs, nanotubes; FTIR, Fourier Transform Infra Red; TEM, transmission electron microscopy; BET, Brunauer Emmett Teller; XRD, X-ray diffraction.

REFERENCES

(1) Bond, G. C.; Thompson, D. T. Gold-Catalysed Oxidation of Carbon Monoxide. *Gold Bull.* **2000**, *33*, 41-50.

(2) Laveille, P.; Biausque, G.; Zhu, H.; Basset, J.-M.; Caps, V. A High-Throughput Study of the Redox Properties of Nb-Ni Oxide Catalysts by Low Temperature CO Oxidation: Implications in Ethane ODH. *Catal. Today* **2013**, *203*, 3-9.

(3) Michel, L., Sall, S., Dintzer, T., Robert, C., Demange, A., and Caps, V. Graphene-Supported 2D Cobalt Oxides for Catalytic Applications. *Faraday Discuss.* **2021**, *227*, 259-273.

(4) Couvret, G.; Genay, G.; Robert, C.; Michel, L.; Caps, V. Intercalation of Copper Phthalocyanine within Bulk Graphite as a New Strategy towards the Synthesis of CuO-based CO Oxidation Catalysts. *Front. Chem.* **2020**, *8*, 735.

(5) Boronat, M.; Corma, A. Molecular Approaches to Catalysis: Naked Gold Nanoparticles as Quasi-Molecular Catalysts for Green Processes. *J. Catal.* **2011**, *284*, 138-147.

(6) Schubert, M.M.; Hackenberg, S.; van Veen, A.C.; Muhler, M.; Plzak, V.; Behm, R.J. CO Oxidation over Supported Gold Catalysts—"Inert" and "Active" Support Materials and Their Role for the Oxygen Supply during Reaction, *J. Catal.* **2001**, *197*, 113-122.

(7) Caps, V.; Arrii, S.; Morfin, F.; Bergeret, G.; Rousset, J.-L. Structures and Associated Catalytic Properties of Well-Defined Nanoparticles Produced by Laser Vaporization of Alloy Rods, *Faraday Discus.* **2008**, *138*, 241-256.

(8) Widmann, D.; Behm, R.J. Active Oxygen on a Au/TiO_2 Catalyst –Formation, Stability and CO Oxidation Activity, *Angew. Chem. Int. Ed.* **2011**, *50*, 10241-10245.

(9) Widmann, D.; Behm, R. J. Activation of Molecular Oxygen and the Nature of the Active Oxygen Species for CO Oxidation on Oxide Supported Au Catalysts. *Acc. Chem. Res.* **2014**, *47*, 740 – 749.

(10) Duan, Z.; Henkelman, G. CO Oxidation at the Au/TiO_2 Boundary: The Role of the Au/Ti5c Site. *ACS Catal.* **2015**, *5*, 1589–1595.

(11) Schlexer, P.; Widmann, D.; Behm, R. J.; Pacchioni, G. CO Oxidation on a Au/TiO_2 Nanoparticle Catalyst via the Au-Assisted Mars–van Krevelen Mechanism. *ACS Catal.* **2018**, *8*, 6513–6525.

(12) Green, I. X.; Tang, W.; Neurock, M.; Yates Jr. J. T. Spectroscopic Observation of Dual Catalytic Sites During Oxidation of CO on a Au/TiO_2 Catalyst. *Science* **2011**, *333*, 736-739.

(13) Wang, Y.-G.; Yoon, Y.; Glezakou, V.-A.; Li, J.; Rousseau, R. The Role of Reducible Oxide–Metal Cluster Charge Transfer in Catalytic Processes: New Insights on the Catalytic Mechanism of CO Oxidation on Au/TiO_2 from ab Initio Molecular Dynamics, *J. Am. Chem. Soc.* **2013**, *135*, 10673–10683.

(14) Wang, Y.; Widmann, D.; Behm, R. J. Influence of TiO_2 Bulk Defects on CO Adsorption and CO Oxidation on Au/TiO_2: Electronic Metal–Support Interactions (EMSIs) in Supported Au Catalysts. *ACS Catal.* **2017**, *7*, 2339–2345.

(15) Costello, C. K.; Kung, M. C.; Oh, H.-S.; Wang, Y.; Kung, H. H. Nature of the Active Site for CO Oxidation on Highly Active Au/γ-Al_2O_3. *Appl. Catal. A* **2002**, *232*, 159–168.

(16) Ivanova, S.; Petit, C.; Pitchon, V.; Caps, V. Support Effects in the Gold-Catalyzed PROX Reaction, *ChemCatChem* **2010**, *2*, 556-563.

(17) Laveille, P.; Guillois, K.; Tuel, A.; Petit, C.; Basset, J.-M.; Caps, V. Durable PROX Catalyst Based on Gold Nanoparticles and Hydrophobic Silica. *Chem. Commun.* **2016**, *52*, 3179-3182.

(18) Vigneron, F.; Caps, V. Evolution in the Chemical Making of Gold Oxidation Catalysts. *C.R. Chimie* **2016**, *19*, 192-198.

(19) Zhang, Y.; Zhang, J.; Zhang, B.; Si, R.; Han, B.; Hong, F.; Niu, Y.; Sun, L.; Li, L.; Qiao, B.; Sun, K.; Huang J.; Haruta, M. Boosting the Catalysis of Gold by O_2 Activation at Au-SiO_2 Interface. *Nat. Commun.* **2020**, *11*, 558.

(20) Daté, M.; Haruta M. Moisture Effect on CO Oxidation over Au/TiO_2 Catalyst. *J. Catal.* **2001**, *201*, 221-224.

(21) Daté, M.; Okumura, M.; Tsubota, S.; Haruta M. Vital Role of Moisture in the Catalytic Activity of Supported Gold Nanoparticles. *Angew. Chem. Int. Ed.* **2004**, *43*, 2129-2132.

(22) Saavedra, J.; Doan, H. A.; Pursell, C. J.; Grabow, L. C.; Chandler, B. D. The Critical Role of Water at the Gold-Titania Interface in Catalytic CO Oxidation, *Science* **2014**, *345*, 1599-1602.

(23) Saavedra, J.; Pursell, C. J.; Chandler B. D. CO Oxidation Kinetics over Au/TiO_2 and Au/Al_2O_3 Catalysts: Evidence for a Common Water-Assisted Mechanism. *J. Am. Chem. Soc.* **2018**, *140*, 3712–3723.

(24) Kung, M. C.; Davis, R. J.; Kung, H. H. Understanding Au-Catalyzed Low-Temperature CO Oxidation, *J. Phys. Chem. C* **2007**, *111*, 11767–11775.

(25) Donoeva, B.; Masoud, N.; de Jongh, P.E. Carbon Support Surface Effects in the Gold-Catalyzed Oxidation of 5-Hydroxymethylfurfural. *ACS Catal.* **2017**, *7*, 4581-4591.

(26) Singh, J. A.; Overbury, S. H.; Dudney, N. J.; Li, M.; Veith, G. M. Gold Nanoparticles Supported on Carbon Nitride: Influence of Surface Hydroxyls on Low Temperature Carbon Monoxide Oxidation. *ACS Catal.* **2012**, *2*, 1138–1146.

(27) Yang, K.; Meng, C.; Lin, L.; Peng, X.; Chen, X.; Wang, X.; Dai, W.; Fu, X. Heterostructured TiO_2–C_3N_4 Support for Gold Catalysts: a Superior Preferential Oxidation of CO in the Presence of H2 under Visible Light Irradiation and without Visible Light Irradiation. *Catal. Sci. Technol.* **2016**, *6*, 829-839.

(28) Huang, Z.; Sun, Q.; Lv, K.; Zhang, Z.; Li, M.; Li, B. Effect of Contact Interface between TiO_2 and g-C_3N_4 on the Photoreactivity of g-C_3N_4/TiO_2 Photocatalyst: (0 0 1) vs (1 0 1) Facets of TiO2. *Appl. Catal. B* **2015**, *164*, 420-427.

(29) Yan, J.; Wu, H.; Chen, H.; Zhang, Y.; Zhang, F.; Liu, S. F. Fabrication of TiO_2/C_3N_4 Heterostructure for Enhanced Photocatalytic Z-Scheme Overall Water Splitting, *Appl. Catal. B* **2016**, *191*, 130-137.

(30) Chen, X.; Wei, J.; Hou, R.; Liang, Y.; Xie, Z.; Zhu, Y.; Zhang, X.; Wang, H. Growth of g-C_3N_4 on Mesoporous TiO_2 Spheres with High Photocatalytic Activity under Visible Light Irradiation, *Appl. Catal. B* **2016**, *188*, 342-350.

(31) Lu, L.; Wang, G.; Zou, M.; Wang, J.; Li, J. Effects of Calcining Temperature on Formation of Hierarchical TiO_2/g-C_3N_4 Hybrids as an Effective Z-Scheme Heterojunction Photocatalyst. *Appl. Surf. Sci.* **2018**, *441*, 1012-1023.

(32) Zou, Y.; Yang, B.; Liu, Y.; Ren, Y.; Ma, J.; Zhou, X.; Cheng, X.; Deng, Y. Controllable Interface-Induced Co-Assembly toward Highly Ordered Mesoporous Pt@TiO_2/g-C_3N_4 Heterojunctions with Enhanced Photocatalytic Performance. *Adv. Function. Mater.* **2018**, *28*, 1806214.

(33) Malik, R.; Tomer, V. K.; Joshi, N.; Dankwort, T.; Lin, L.; Kienle, L. Au–TiO2-Loaded Cubic g-C_3N_4 Nanohybrids for Photocatalytic and Volatile Organic Amine Sensing Applications. *ACS Appl. Mater. Interfaces* **2018**, *10*, 34087–34097.

(34) Vidyasagar, D.; Balapure, A.; Ghugal, S. G.; Shende, A. G.; Umare, S. S. Template-Free Macro-Mesoporous TiO_2/Carbon Nitride Interface for Visible-Light-Driven Photocatalysis. *Phys. Status Solidi A* **2019**, *216*, 1900212.

(35) Raheman AR, S.; Wilson, H. M.; Momin, B. M.; Annapure, U. S.; Jha. N. TiO2 Nanosheet/Ultra-Thin Layer g-C_3N_4 Core-Shell Structure: Bifunctional Visible-Light Photocatalyst for H_2 Evolution and Removal of Organic Pollutants from Water. *Appl. Surf. Sci.* **2020**, *528*, 146930.

(36) Marchal, C.; Cottineau, T.; Colbeau-Justin, C.; Caps, V.; Keller, V. Au/TiO_2-gC_3N_4 Nanocomposites for Enhanced Photocatalytic H_2 Production from Water under Visible Light Irradiation with Very Low Quantities of Sacrificial Agents, *Adv. En. Mater.* **2018**, *8*, 1702142.

(37) Jiménez-Calvo, P.; Caps, V.; Nawfal Ghazzal, M.; Colbeau-Justin, C.; Keller, V. Au/TiO_2(P25)-gC_3N_4 Composites with Low g-C_3N_4 Content Enhance TiO_2 Sensitization for Remarkable H_2 Production from Water under Visible-Light Irradiation, *Nano Energy* **2020**, *75*, 104888.

(38) Jiménez-Calvo, P.; Marchal, C.; Cottineau, T.; Caps, V.; Keller, V. Influence of the Gas Atmosphere during the Synthesis of g-C_3N_4 for Enhanced Photocatalytic H_2 Production from Water on Au/g-C_3N_4 Composites. *J. Mater. Chem. A* **2019**, *7*, 14849-14863.

(39) Naseem, F.; Lu, P.; Zeng, J.; Lu, Z.; Hau Ng, Y.; Zhao, H.; Du, Y.; Yin, Z. Solid Nanoporosity Governs Catalytic CO_2 and N_2 Reduction. *ACS Nano* **2020**, *14*, 7734–7759.

(40) Kasuga, T.; Hiramatsu, M.; Hoson, A.; Sekino, T.; Niihara, K. Formation of Titanium Oxide Nanotube. *Langmuir* **1998**, *14*, 3160–3163.

(41) Vigneron, F.; Piquet, A.; Baaziz, W.; Ronot, P.; Boos, A.; Janowska, I.; Pham-Huu, C.; Petit, C.; Caps, V. Hydrophobic Gold Catalysts: from Synthesis on Passivated Silica to Synthesis on Few-Layer Graphene. *Catal. Today* **2014**, *235*, 90-97.

(42) Marchal, C.; Behr, M.; Vigneron, F.; Caps, V.; Keller, V. Au/TiO_2 Photocatalysts Prepared by Solid Grinding for Solar-Light Water Splitting. *New J. Chem.* **2016**, *40*, 4428-4435.

(43) Thommes, M.; Kaneko, K.; Neimark, A. V.; Olivier, J. P.; Rodriguez-Reinoso, F.; Rouquerol J.; Sing, K. S. W. Physisorption of Gases, with Special Reference to the Evaluation of Surface

Area and Pore Size Distribution (IUPAC Technical Report). *Pure Appl. Chem.* **2015**, *87*, 1051-1069; Bardestani, R.; Patience G. S.; Kaliaguine, S. Experimental Methods in Chemical Engineering: Specific Surface Area and Pore Size Distribution Measurements—BET, BJH, and DFT. *Can. J. Chem. Eng.* **2019**, *97*, 2781–2791.

(44) Rasband, W. http://rsb.info.nih.gov/ij/

(45) Zhong, L.P.; Barreau, M.; Caps, V.; Papaefthimiou, V.; Hae vecker, M.; Teschner, D.; Baaziz, W.; Borfecchia, E.; Braglia, L.; Zafeiratos, S. Improving the Catalytic Performance of Cobalt for CO Preferential Oxidation by Stabilizing the Active Phase through Vanadium Promotion. *ACS Catal.* **2021**, *11*, 5369-5385.

(46) Zhong, L.; Barreau, M.; Chen, D.; Caps, V.; Haevecker, M.; Teschner, D.; Simonne, D. H.; Borfecchia, E.; Baaziz, W.; Šmíd, B.; Zafeiratos, S. Effect of Manganese Promotion on the Activity and Selectivity of Cobalt Catalyst for CO Preferential Oxidation, *Appl. Catal. B* **2021**, *297*, 120397.

(47) Van Hardeveld, R.; Hartog, F. The Statistics of Surface Atoms and Surface Sites on Metal Crystals. *Surf. Sci.* **1969**, *15*, 189-230.

(48) Ahmed, S.; Ramli, A.; Yusup S.; Farooq, M. Adsorption Behavior of Tetraethylenepentamine-Functionalized Si-MCM-41 for CO_2 Adsorption. *Chem. Eng. Res. Des.* **2017**, *122*, 33-42.

(49) Dong, F.; Li, Y.; Wang, Z.; Ho, W.-K. Enhanced Visible Light Photocatalytic Activity and Oxidation Ability of Porous Graphene-Like g-C_3N_4 Nanosheets via Thermal Exfoliation. *Appl. Surf. Sci.* **2015**, *358*, 393–403.

(50) Zhang, J.-B.; Tan, Z.-C.; Meng, S.-H.; Li, S.-H.; Zhang, L.-M. Heat Capacity and Thermal Decomposition of Dicyandiamide. *Thermochimica Acta* **1997**, *307*, 1-15.

(51) Raskó, J.; Bánsági, T.; Solymosi, F. HCN Adsorption on Silica and Titania Supported Rh Catalysts Studied by FTIR. *Phys. Chem. Chem. Phys.* **2002**, *4*, 3509–3513.

(52) Lin, Y.-C.; Chien, T.-E.; Li, K.-L.; Lin, J.-L. Comparison of the Thermal and Photochemical Reaction Pathways of Melamine on TiO_2, *J. Phys. Chem. C* **2015**, *119*, 8645–8651.

(53) Chen, X.; Xie, Z.; Liang, Y.; Wei, J.; Zhu, Y.; Huo, Y.; Zhang, X.; Wang, H. Hybridizing TiO_2 with Nitrogen-Doped Carbon: A New Route to A Highly Visible Light-Active Photocatalyst. *ChemistrySelect* **2017**, *2*, 1565 – 1572.

(54) Kerdi, F.; Caps, V.; Tuel, A. Innovative Preparation of Au/C by Replication of Gold-containing Mesoporous Silica Catalysts, *Stud. Surf. Sci. Catal.* **2010**, *175*, 221-224.

(55) Kerdi, F.; Caps, V.; Tuel, A. Mesostructured Au/C Materials Obtained by Replication of Functionalized SBA-15 Silica Containing Highly Dispersed Gold Nanoparticles, *Micropor. Mesopor. Mater.* **2011**, *140*, 89-96.

(56) Martha, S.; Nashim, A.; Parida, K. M. Facile Synthesis of Highly Active g-C_3N_4 for Efficient Hydrogen Production under Visible Light. *J. Mater. Chem. A* **2013**, *1*, 7816-7824.

(57) Bojdys, M. J.; Muller, J.-O.; Antonietti, M.; Thomas, A. Ionothermal Synthesis of Crystalline, Condensed, Graphitic Carbon Nitride. *Chem. Eur. J.* **2008**, *14*, 8177-8182.

(58) Caps, V.; Tsang, S. C. Heterogenisation of Os Species on MCM-41 Structure for Epoxidation of *trans*-Stilbene. *Appl. Catal. A* **2003**, *248*, 19-31.

(59) Cho, H.-G.; Andrews, L. Infrared Spectra of $CH_2dM(H)NC$, CH_3-MNC, and η^2-M(NC)-CH_3 Produced by Reactions of Laser-Ablated Group 5 Metal Atoms with Acetonitrile. *J. Phys. Chem. A* **2010**, *114*, 5997–6006.

(60) Lu, P.; Wang, Y. The Thriving Chemistry of Ketenimines. *Chem. Soc. Rev.* **2012**, *41*, 5687–5705.

(61) Jacox, M. E. Matrix Isolation Study of the Interaction of Excited Argon Atoms with Methyl Cyanide. Vibrational and Electronic Spectra of Ketinimine. *Chem. Phys.* **1979**, *43*, 157-172.

(62) Jacox, M. E.; Milligan D.E. Infrared Study of the Reactions of CH2 and NH with C2H2 and C2H4 in Solid Argon. *J. Am. Chem. Soc.* **1963**, *85*, 278-282.

(63) Ishida, T.; Murayama, T.; Taketoshi, A.; Haruta, M. Importance of Size and Contact Structure of Gold Nanoparticles for the Genesis of Unique Catalytic Processes. *Chem. Rev.* **2020**, *120*, 464-525.

(64) Johnston, L. J.; de Mayo, P.; Wong. S. K. Surface Photochemistry: Decomposition of Azobis(isobutyronitrile) on Dry Silica Gel. *J. Org. Chem.* **1984**, *49*, 20-26.

(65) Caps, V.; Wang, Y.; Gajecki, J.; Jouguet, B.; Tuel, A.; Morfin, F.; Rousset, J.L. Effect of the Titania Morphology on the Preparation of Au/TiO_2(/SiO_2) Catalysts. *Stud. Surf. Sci. Catal.* **2006**, *162*, 127-134.

(66) Quinet, E.; Morfin, F.; Diehl, F.; Avenier, P.; Caps, V.; Rousset, J.-L. Hydrogen Effect on the Preferential Oxidation of Carbon Monoxide over Alumina-Supported Gold Nanoparticles, *Appl. Catal. B* **2008**, *80*, 195-201.

(67) Quinet, E.; Piccolo, L.; Daly, H.; Meunier, F. C.; Morfin, F.; Valcarcel, A.; Diehl, F.; Avenier, P.; Caps, V.; Rousset, J.-L. H_2-Induced Promotion of CO Oxidation over Unsupported Gold, *Catal. Today* **2008**, *138*, 43-49.

Authors are required to submit a graphic entry for the Table of Contents (TOC) that, in conjunction with the manuscript title, should give the reader a representative idea of one of the following: A key structure, reaction, equation, concept, or theorem, etc., that is discussed in the manuscript. Consult the journal's Instructions for Authors for TOC graphic specifications.